

Large-area fabrication of high aspect ratio tantalum photonic crystals for high-temperature selective emitters

Veronika Rinnerbauer, Sidy Ndao, Yi Xiang Yeng, Jay J. Senkevich, Klavs F. Jensen et al.

Citation: *J. Vac. Sci. Technol. B* **31**, 011802 (2013); doi: 10.1116/1.4771901

View online: <http://dx.doi.org/10.1116/1.4771901>

View Table of Contents: <http://avspublications.org/resource/1/JVTBD9/v31/i1>

Published by the AVS: Science & Technology of Materials, Interfaces, and Processing

Related Articles

Simulation study of cleaning induced extreme ultraviolet reflectivity loss mechanisms on mask blanks

J. Vac. Sci. Technol. B **30**, 051604 (2012)

Application of GaInNAs for the gain medium of a photonic crystal microcavity

J. Vac. Sci. Technol. B **30**, 02B127 (2012)

Coexistence of guided mode resonance and extraordinary optical transmission in metal/dielectric/metal photonic crystal slab

J. Vac. Sci. Technol. B **29**, 06FF05 (2011)

Probe field enhancement in photonic crystals by upconversion nanoparticles

J. Vac. Sci. Technol. B **29**, 06F403 (2011)

Releasable infrared metamaterials

J. Vac. Sci. Technol. B **29**, 051806 (2011)

Additional information on *J. Vac. Sci. Technol. B*

Journal Homepage: <http://avspublications.org/jvstb>

Journal Information: http://avspublications.org/jvstb/about/about_the_journal

Top downloads: http://avspublications.org/jvstb/top_20_most_downloaded

Information for Authors: http://avspublications.org/jvstb/authors/information_for_contributors

ADVERTISEMENT

Instruments for advanced science



Gas Analysis

- dynamic measurement of reaction gas streams
- catalysis and thermal analysis
- molecular beam studies
- dissolved species probes
- fermentation, environmental and ecological studies



Surface Science

- UHV TPD
- SIMS
- end point detection in ion beam etch
- elemental imaging - surface mapping



Plasma Diagnostics

- plasma source characterization
- etch and deposition process reaction kinetic studies
- analysis of neutral and radical species



Vacuum Analysis

- partial pressure measurement and control of process gases
- reactive sputter process control
- vacuum diagnostics
- vacuum coating process monitoring

contact Hiden Analytical for further details



info@hideninc.com
www.HidenAnalytical.com
 CLICK to view our product catalogue 

Large-area fabrication of high aspect ratio tantalum photonic crystals for high-temperature selective emitters

Veronika Rinnerbauer,^{a)} Sidy Ndao, Yi Xiang Yeng, Jay J. Senkevich, Klavs F. Jensen, John D. Joannopoulos, Marin Soljačić, and Ivan Celanovic
Massachusetts Institute of Technology, Cambridge, Massachusetts 02139

Robert D. Geil

Institute of Advanced Materials, University of North Carolina, Chapel Hill, North Carolina 27599

(Received 28 September 2012; accepted 27 November 2012; published 12 December 2012)

The authors present highly selective emitters based on two-dimensional tantalum (Ta) photonic crystals, fabricated on 2 in. polycrystalline Ta substrates, for high-temperature applications, e.g., thermophotovoltaic energy conversion. In this study, a fabrication route facilitating large-area photonic crystal fabrication with high fabrication uniformity and accuracy, based on interference lithography and reactive ion etching is discussed. A deep reactive ion etch process for Ta was developed using an SF₆/C₄F₈ based Bosch process, which enabled us to achieve ~ 8.5 μm deep cavities with an aspect ratio of ~ 8 , with very steep and smooth sidewalls. The thermal emitters fabricated by this method show excellent spectral selectivity, enhancement of the emissivity below cut-off approaching unity, and a sharp cut-off between the high emissivity region and the low emissivity region, while maintaining the low intrinsic emissivity of bare Ta above the cut-off wavelength. The experimental results show excellent agreement with numerical simulations.

© 2013 American Vacuum Society. [<http://dx.doi.org/10.1116/1.4771901>]

I. INTRODUCTION

The ability to tailor the photonic density of states and thereby thermal radiation in photonic crystals (PhCs) enables the efficient design of highly selective and efficient thermal radiation sources. Metallic PhCs are promising as high performance selective thermal emitters for solid-state thermal-to-electricity energy conversion concepts including thermophotovoltaic (TPV) energy conversion,^{1,2} as well as highly selective solar absorbers/emitters for solar thermal and solar TPV applications.³

Two-dimensional all-metallic PhCs from refractory metals are particularly suitable for high-temperature applications, since they offer superior thermomechanical and thermochemical stability as opposed to multilayer and multi-material structures or metal-dielectric composite coatings.^{4–8} Also, the design route based on fundamental principles of the 2D PhCs facilitates very good control over the emissivity and its cut-off wavelength.

Recent work on tungsten (W) PhCs^{9–15} for high-temperature applications demonstrated very promising results regarding selective thermal emitters and absorbers. In particular, 2D PhCs on W fabricated by comparably expensive and time-consuming electron-beam (e-beam) lithography have been reported by Sai *et al.*^{10,11} Also, 3D structures like inverse opal PhCs were reported in Refs. 16 and 17 and 3D woodpile PhCs fabricated by direct laser writing in Ref. 18 and by a layer-by-layer fabrication, reported in Refs. 19 and 20. For target applications in solid-state energy conversion, we focus on a fabrication route based on interference lithography (IL), as proposed in Refs. 9 and 13–15, that facilitates large-area ($\gg 1$ cm²) fabrication of 2D PhCs and ensures fabrication uniformity and accuracy over large areas.

We propose an approach based on polycrystalline tantalum (Ta), which has a high melting point (3290 K) and low vapor pressure similar to W as well as good intrinsic selective emissivity, with long wavelength emissivity (above ~ 2 μm) even below that of W. Moreover, Ta is weldable and machinable, which allows for easy integration into any device design, e.g., for energy conversion applications based on solar-, radioisotope-, and combustion-TPV. However, single crystal Ta is only available in small sizes (~ 1 cm diameter) and the cost is prohibitive for any practical application. Therefore, we use high-purity polycrystalline Ta of up to 2 in. diameter for our substrates, paving the way to large scale emitters. Furthermore, we found that annealing polycrystalline Ta produces large grains, which increases material stability and minimizes grain boundaries, thus improving the optical properties and their high-temperature stability.

We demonstrate a fabrication route for Ta PhCs, based on a square array of cylindrical cavities, and fabricated selective emitters on 2 in. diameter polycrystalline substrates. We use standard microfabrication processes that allow for easy scaling to larger substrates. Moreover, we established a deep reactive ion etch (DRIE) process for Ta, using an SF₆ based Bosch process. As Ta has low emissivity in the near IR, the PhC needs deep cavities (> 5 μm) to enable efficient absorption, i.e., enhancement of the emissivity below the cut-off wavelength.²¹ With the optimized process parameters, we achieved deep (up to ~ 8.5 μm), high aspect ratio cavities (up to ~ 8), very steep and smooth side walls, and extremely high etch selectivity (at least 1:200) with respect to the hard Cr etch mask.

Measurements of fabricated high aspect ratio Ta PhCs show enhancement of the emissivity at wavelengths below cut-off wavelength approaching that of blackbody, steep cut-off between high and low emissivity spectral regions, and a

^{a)}Electronic mail: vrinner@mit.edu

high level of spectral selectivity, in very good agreement with theoretical results from numerical simulations.

II. MATERIALS AND FABRICATION

A. Substrate preparation

Substrates of 3/4 in. (1.9 cm) and 2 in. (5 cm) diameter, and 3 mm thickness made from high purity (>99.9%) polycrystalline Ta (Rembar) were used to fabricate 2D PhCs for selective emitters. Essential to the PhC fabrication is the flatness, small surface roughness, large grain size, and high thermal stability of the Ta substrate. Polycrystalline Ta is more affordable and readily available in large-area substrates as opposed to single crystal substrates. On the other hand, polycrystalline metals typically have grain sizes that are smaller or comparable to the feature size of PhC and are much less thermally stable than single crystals. Small grain size is detrimental to the performance of high-temperature nanophotonic devices for two reasons: first, small grain size on the order of the PhC feature sizes could interfere with PhC pattern and lead to poor optical performance, and second, polycrystalline material is thermodynamically unstable at high temperatures, and hence grain boundary migration and grain growth could lead to disintegration of the PhC structure. Therefore, large grain size (\gg feature size) substrates are critical as a starting point for high-temperature nanophotonics and preannealing of the polycrystalline substrates at high temperature can enhance thermal stability by preventing recrystallization and grain migration at high operating temperatures.

To prepare substrates for nanofabrication, the polycrystalline substrates were cut, lapped, and annealed at 2250 °C under vacuum for 4 h. After annealing, the substrates showed a bifurcated grain structure with large grains on the order of 1–2 mm across and small grains of 0.1–0.5 mm across. The boundaries of the large grains were as deep as 200 nm as determined by AFM, whereas the depth of the smaller grain boundaries was comparable to the surface roughness. The substrates were subsequently lapped and polished to an optical degree with a surface roughness of $R_a < 1$ nm and a flatness and parallelism on the order of 2.5 and 12.5 μ m, respectively.

B. Fabrication

A square array of circular cavities was etched into the annealed and polished Ta substrates to fabricate the selective emitters, using a process similar to that used for W PhCs,^{14,15} albeit with some changes optimized for Ta substrates and large-area fabrication. The fabrication of the PhCs comprises the steps of pattern definition by interference lithography based on a trilayer resist process,^{22,23} definition of the cavity diameter by isotropic plasma ashing, pattern transfer to a thin chrome (Cr) hard mask by reactive ion etching (RIE), and the final etching of the substrate. Figure 1 shows the schematic outline of the fabrication process. The dry etch process of the Cr hard mask was chosen over the less complex wet etch of Cr, as it yields the advantages of eliminating random edge roughness of the Cr cavity and providing superior control over the cavity diameter.

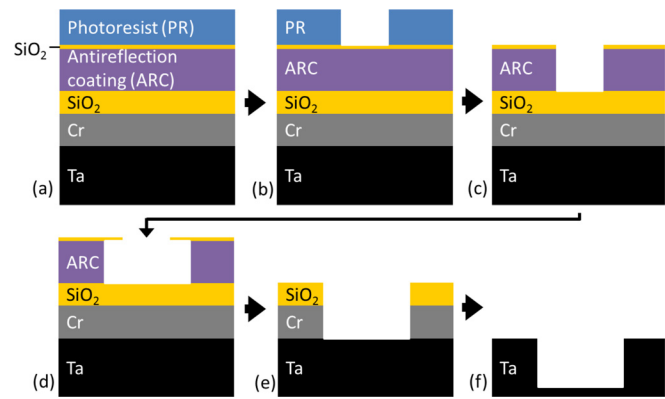


Fig. 1. (Color online) Schematic outline of the process flow: (a) Deposition of the mask layers for lithography and etching, (b) pattern definition by lithography and removing of developed photoresist, (c) pattern transfer into first SiO₂ and ARC layers by RIE, (d) definition of hole diameter by plasma ashing of the ARC, (e) pattern transfer into the second SiO₂ and Cr hard mask by RIE, (f) final etching of Ta by DRIE.

To define the etch mask for the Ta substrate, a thin layer of Cr followed by a layer of SiO₂ is deposited on the Ta substrate by e-beam evaporation for the definition of the hard etch mask. It was shown that 50 nm of Cr is sufficient to achieve up to 8.5 μ m deep cavities in the DRIE etch. For the SiO₂ layer, which serves as a mask for the dry etch of Cr, a layer thickness of about half of that of the Cr layer is sufficient. This is followed by the deposition of the three layers necessary for IL: a layer of antireflection coating (ARC, AZ BARLi) of about 270 nm was spincoated on top of the SiO₂, followed by a 10 nm thick SiO₂ layer deposited by e-beam evaporation, and finally spin coating of negative photoresist (THMR-iNPS4, OHKA America) for the lithography, with a thickness of about 250 nm. The ARC serves to reduce reflection from the substrate and formation of vertical standing waves during interference lithography.^{22,23} An ARC thickness of about 270 nm results not in the absolute minimum of reflection on our samples, but in a broadband low reflectivity of less than 5% for a broad range of SiO₂ layer thicknesses (0–100 nm). The SiO₂ layer on top of the ARC is used as a protection layer when etching and ashing the ARC.

After deposition of the mask layers, laser IL is used to define the periodic pattern. IL is a relatively inexpensive, fast and precise maskless lithography method, which relies on the interference pattern generated by two coherent light sources to define 1D and 2D periodic patterns in a single plane, and is easily scalable to large exposure areas. The photoresist is exposed either in a Lloyd's mirror IL system (for small substrates)²⁴ or in an achromatic Mach-Zehnder IL system,^{25,26} both using a 325 nm HeCd Laser. The periodicity of the pattern is defined by the interference angle, and the exposure is performed twice, with the substrates rotated by 90° between exposures to create a square array of cylindrical cavities. In the Lloyd's mirror IL setup, the exposed area is limited by the size of the mirror creating the second laser beam and the chosen interference angle, in our case to a square of about 1/2 in. side length. In contrast, the Mach-Zehnder IL setup allows for large exposure areas, facilitating

easy upscaling of the fabrication process to larger substrate sizes. Due to the distribution of the intensity in the plane of the substrate, the diameter of the nonexposed circular areas increases from the center to the edge of the exposed area, causing a slight variation of the cavity diameter.

Generally, when IL is used to pattern a photoresist, the lines of high and low intensity radiation are equally spaced. To achieve round holes rather than square ones in the exposed photoresist, the exposure dose can be increased, which results in round holes due to the proximity effect, but also decreases the hole diameter further. Therefore, the cavities defined by IL typically have a diameter-to-period ratio of 0.3–0.45. The design of the Ta PhC, in contrast, calls for a higher diameter-to-period ratio of at least 0.75 to achieve a broadband high emissivity range in the near IR. The target diameter for a cut-off wavelength of $2.0\ \mu\text{m}$ is $1.08\ \mu\text{m}$ and the target period $1.3\ \mu\text{m}$ in our optimized design (see Sec. III A). Accordingly, the diameter of the cavities defined in negative resist by IL has to be increased substantially (by $\geq 500\ \text{nm}$) in the subsequent steps transferring the pattern to the Cr hard mask. This is achieved in two steps by isotropic plasma ashing of both the photoresist as well as the ARC. The exposed photoresist is developed in commercial CD-26 and then partially removed in an O_2 plasma asher. The maximum achievable increase in hole diameter in this step is limited by the resist thickness, with enough resist left to transfer the pattern into the underlying layers. Typically, an increase in hole diameter of about $200\ \text{nm}$ can be achieved by ashing for $90\ \text{s}$ at $200\ \text{W}$. After ashing of the resist, the pattern is transferred into the SiO_2 and ARC layers by CHF_3 and He/O_2 based RIE processes, respectively, using a Plasmatherm 790. The etch parameters are given in Table I. Subsequently, the hole diameter is increased more by plasma ashing the ARC layer to the final diameter. Since the ARC is protected by the SiO_2 layer, which is not damaged by the O_2 plasma, even large diameter-to-period ratios can be achieved by this step (see Fig. 2). In Fig. 2, scanning electron microscope (SEM) images of the samples at different stages during the process illustrate the different fabrication steps of the lithography and mask layer structuring. Note that the cross-sectional views are taken from Si control samples processed in the same way, since the Ta substrates are not cut or cleaved easily and these fabrication steps are independent of the substrate material.

TABLE I. Parameters used in RIE etch steps.

Material ^a	Gases	Flow (sccm)	Pressure (mTorr)	Power (W)
ARC ¹	He/O_2	10/5	7	80
SiO_2	CHF_3	15	10	90
Cr ²	Cl_2/O_2	15/3	5	300/100 substrate (RF)
Ta ³	$\text{SF}_6/\text{C}_4\text{F}_8$	200/100	3	1200/75 substrate (LF)

^aSystem: 1–Plasmatherm 790, 2–Nexx Cirrus 150, 3–Alcatel AMS100.

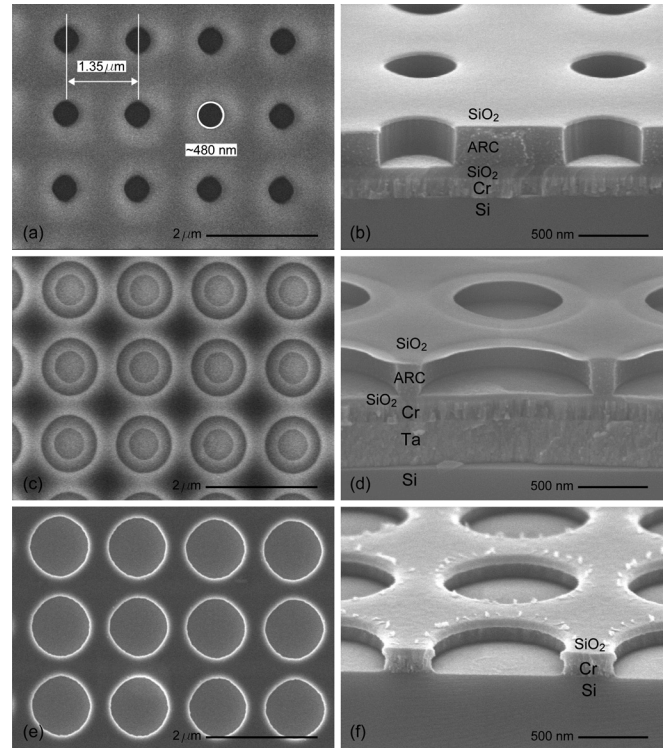


Fig. 2. Scanning electron micrographs of the fabrication steps for the Ta PhC: (a) developed photoresist after IL, (b) lithography layers (SiO_2 and ARC) etched by RIE, (c) and (d) definition of hole diameter by plasma ashing of the ARC, (e) and (f) pattern transfer into Cr hard mask by RIE. (Cross sections are taken of a cleaved Si control sample for the presented fabrication steps, which do not depend on the substrate material.)

Opening of the cavities by ashing enables us to achieve smooth sidewalls of the cavities, which are transferred to the Cr hard mask by dry etching and subsequently into the Ta. This is a major advantage as compared to a chemical wet etch of the Cr mask (as employed before for W PhCs^{14,15}) which results in substantial sidewall roughness and poor control over cavity diameter, often leading to broken sidewalls between cavities. Figures 3(a) and 3(b) compare cavities in Ta achieved using the Cr wet etch and the dry etch (RIE), respectively. We have also investigated the effect of stochastic sidewall roughness on the optical properties by numerical simulations, as shown in Fig. 3(c). With increasing roughness the Q-factor of the cavity resonances decreases, resulting in slightly decreased emissivity contrast between short and long-wavelength region decreases. At the same time, even for constant cavity area in the simulations, the effective radius of the structure increases and the cut-off shifts to larger wavelengths. Finally, as sidewalls are breaking, cavities may become connected, allowing interaction with electromagnetic waves of larger wavelength. As the emissivity cut-off is defined by the fundamental mode of the cavity,^{11,13,15,27,28} the emissivity at long wavelengths increases dramatically in this case, and the desired selectivity is lost.

Once the desired diameter is obtained, the cavities are etched into the underlying SiO_2 layer by the same CHF_3 based RIE process, and subsequently into the Cr layer by a Cl_2/O_2 based RIE process using a Nexx Cirrus 150, with the

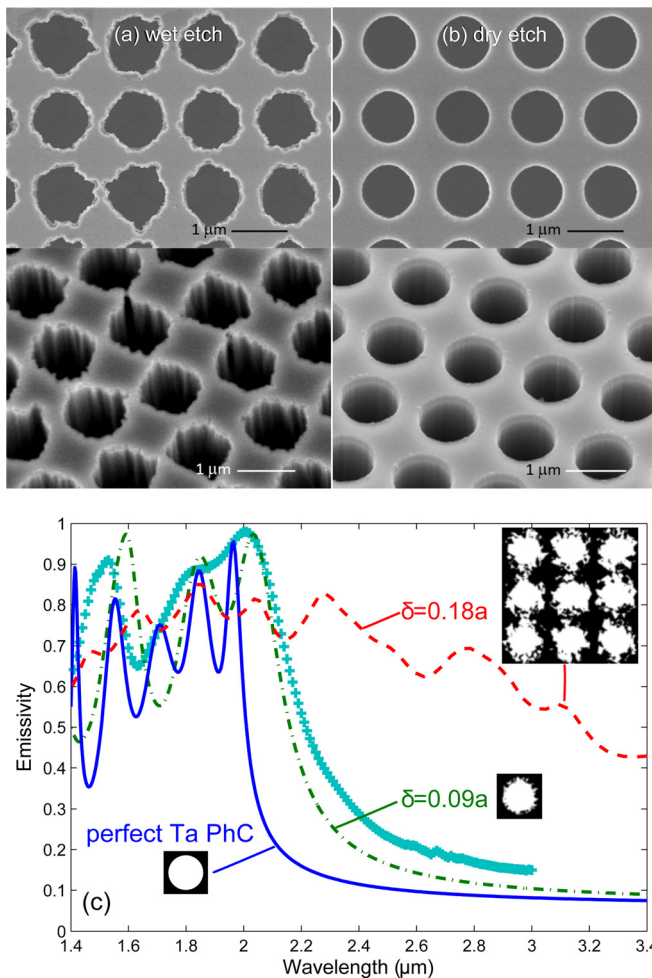


Fig. 3. (Color online) (a) and (b) Scanning electron micrographs of fabricated Ta PhC obtained by chemical wet etch and dry etch (RIE) of the Cr mask, respectively. (c) Simulation of the emissivity for a Ta PhC with perfect structure (solid line) and increasing sidewall roughness characterized by the maximum deviation $\delta = 0.09a$ (dashed-dotted line) comparable to the PhC fabricated by wet etch with the measured emissivity (crosses), and simulation with $\delta = 0.18a$ (dashed line) resulting in breaking sidewalls.

SiO₂ serving as an etch mask for the Cr. The Cr etch process was optimized to achieve an anisotropic etch with straight sidewalls, which is facilitating the subsequent Ta DRIE step. Table I lists the respective parameters for the RIE etch steps.

Finally, the pattern has to be transferred to the Ta substrate by a DRIE step to achieve deep cavities. We established a SF₆/C₄F₈ based Bosch process to etch the Ta, using an Alcatel AMS100 DRIE. The process parameters of this step were optimized for deep cavities in Ta and maximum sidewall straightness, using the following values: SF₆ (200 sccm)/C₄F₈ (100 sccm) with 3 s/1.5 s pulses, respectively, power 1200 W, pressure ~ 3 mT, substrate bias 75 W, and temperature 20 °C. For these process parameters, we achieve an etch rate of approximately 14 nm/s for Ta. The pulse duration of the etch step (SF₆) and passivation step (C₄F₈) was optimized to 3:1.5 to achieve complete passivation of the sidewalls. To achieve straight sidewalls, it is imperative to keep the substrate temperature low; therefore, repeated short etch steps of maximum 5 min duration were used. With this process we have been

able to achieve up to ~ 8.5 μm deep cavities with an aspect ratio of up to ~ 8 , very steep sidewalls and negligible sidewall roughness, and very good etch selectivity. The selectivity of the Ta etch step is high enough that a layer of 50 nm of Cr is sufficient to achieve this etch depth, with the Cr layer thickness hardly reduced by the etch, so the selectivity amounts to at least 200.

After DRIE of Ta, the remaining Cr layer is removed completely by immersion into Cr-7 (Cyantek) liquid etchant. The remains of a thin passivation layer on the sidewalls of the cavities from the DRIE etching of the Ta do not influence the optical properties of the photonic crystal.

III. DESIGN AND CHARACTERIZATION

A. Design

The flexible design approach based on the fundamental principles of the PhC^{15,28} facilitates efficient tailoring of the cut-off wavelength of the emissivity, e.g., to match it to the bandgap λ_{PV} of a PV cell for TPV applications. By creating cavity modes and careful matching of the quality (Q) factors of the radiative and absorbing modes of the cavities of the PhC,^{15,28} the emissivity below the cut-off wavelength is greatly increased from the intrinsic emission of flat Ta, approaching that of a blackbody. At the same time, the emission at wavelengths above cutoff, with wavelengths longer than the fundamental cavity mode and therefore forbidden from entering the cavity, is kept low, approaching that of the bare substrate for long wavelengths, and high selectivity with a sharp cutoff between the two regions is achieved. We employ a finite difference time domain (FDTD) algorithm²⁹ implemented via MEEP,³⁰ a freely available software package developed at MIT, for simulation of the optical properties of the PhCs, which are designed as a square array of circular cavities with a period a , radius r , and cavity depth d etched into the substrate (see inset in Fig. 5). The optical dispersion relation of Ta is incorporated in the simulations via a Lorentz–Drude oscillator model, whose parameters are fitted to the experimentally measured reflectance of flat polished Ta.

As an example, we designed and fabricated a Ta PhC for a cut-off wavelength of $\lambda_{PV} = 2.0$ μm (corresponding to a bandgap of 0.62 eV). The parameters of the PhC were optimized to achieve a spectral emissivity approaching an ideal step-function with this cut-off wavelength, resulting in an optimized cavity radius $r = 0.54$ μm, a period $a = 1.3$ μm, and an etch depth $d = 8.0$ μm.²¹ As the emissivity of bare Ta below this cut-off wavelength is low, the PhC needs deep cavities to achieve a high quality factor Q of the fundamental cavity resonant mode, and a long interaction time of the radiation in this mode to be efficiently absorbed, to achieve a strong increase in emissivity. To facilitate fabrication, the etch depth of the cavities was limited to 8 μm in the optimization. Simulations have shown that for increased cavity depth above $\sim d = 8.0$ μm, the benefit of increased selectivity of the emissivity is diminishing. A sharp cutoff between the high emissivity range approaching unity and the low emissivity range, limited by the intrinsic emissivity of Ta, can be achieved even for this etch depth.

Note that the simulated emissivity is for normal incidence. There is an angular dependence of the emissivity and thereby also the emission for 2D PhC, as studied in detail in Yeng *et al.*¹⁵ and Bermel *et al.*³¹ With increasing incident angle, not only the cutoff shifts slightly but also the coupling strength of the cavity modes, which are the origin for increased emissivity below the cutoff of the fundamental cavity mode, decreases. At glazing incidence, finally the emissivity approaches that of the flat substrate. This angular dependence can be used to advantage in selective solar absorbers based on 2D metallic PhCs, using angular selectivity as a means of concentration.³¹ In selective emitters for TPV systems with large view factors, i.e., small distance between the emitter and the TPV cell, angular dependence of the emission is undesirable and a large drop of spectral selectivity with emission angle would decrease system performance. Therefore, the angular dependency of the PhC has to be taken into account when optimizing the structure for an application or a specific system.¹⁵

B. Characterization

Figure 4 shows scanning electron micrographs of the fabricated Ta PhCs. The fabricated samples exhibit features sizes very close to the target parameters with diameters of about $1.08\ \mu\text{m}$, periods of about $1.35\ \mu\text{m}$. The etch depth obtained on different samples is approximately $6\text{--}8.5\ \mu\text{m}$. The etch depth is estimated from SEM images of the cross section at a defect site (Fig. 4 inset), as the sample cannot be cleaved or cut easily, and the aspect ratio of the cavities is too high for AFM measurements.

The spectral emissivity of fabricated Ta PhCs is obtained from near normal incidence reflectivity measurements at room temperature. The reflectivity measurement is performed using a quartz halogen lamp as a white light source in conjunction with a monochromator, an optical setup providing an incident angle of 15° on the sample and a PbS photodetector. The measurement is calibrated against a known aluminum mirror in the range of $1\text{--}3\ \mu\text{m}$. As the samples are

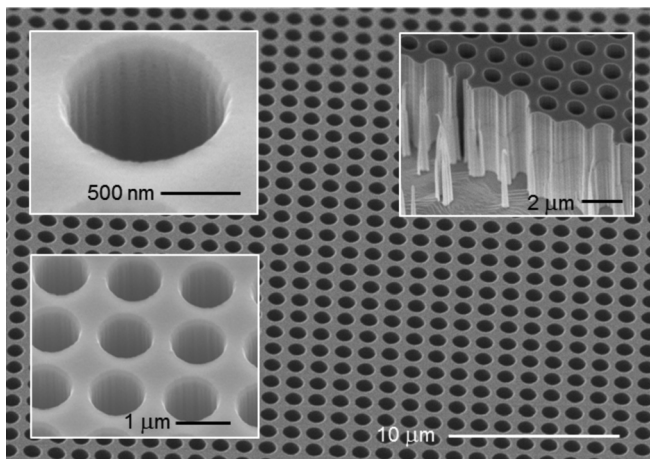


Fig. 4. Scanning electron micrographs of fabricated Ta PhC showing excellent fabrication accuracy and long range fabrication uniformity. Left insets: Close-up of etched cavities (with remaining Cr mask on top). Right inset: Cross-sectional view of the etched Ta PhC.

opaque, transmission is zero and according to Kirchhoff's law the emissivity E and the reflectivity R amount to unity for every wavelength; therefore, $E = 1 - R$. The emissivity of a Ta PhC fabricated on a 2 in. diameter substrate is shown in Fig. 5, and a digital photo of the full 2 in. PhC is shown in the inset. As can be seen, there is a substantial increase of the emissivity below the cutoff at $2\ \mu\text{m}$ as compared to that of flat Ta, while the emissivity above the cutoff is kept low. A sharp cutoff between high and low emissivity regions is achieved, offering a 4:1 emissivity contrast over a wavelength range of 10%.

As discussed, there is a variation of the cavity diameter that is intrinsic to the use of IL on large-area substrates. This variation results in $\sim 20\ \text{nm}$ or $\Delta 2r = 1.9\%$ increase of the diameter of the final cavities from the center to the edge of the 2 in. substrate. Correspondingly, the cut-off wavelength shifts by $\sim 40\ \text{nm}$ or $\Delta \lambda = 2\%$ to longer wavelengths when measured in the center or on the edge of the substrate (see inset of Fig. 5). We also demonstrated the fabrication of the PhC in the Cr hard mask on a 4 in. Si wafer using the same process. In this case, the variation of the cavity diameter was $\sim 80\ \text{nm}$ or $\Delta 2r = 7\%$ from the center to the edge of the 4 in. wafer.

Studies of the influence of various fabrication imperfections show that for the fabricated samples, a very slight broadening of the measured cutoff is mostly due to a slight tapering in the sidewall profile, which results in a vertically decreasing cavity radius and smaller effective radius and therefore a shift of the first resonance peak to shorter wavelengths with a less steep cutoff. Sidewall disorder, i.e., random roughness of the cavity edge can be neglected due to our optimized dry etch process of the Cr hard mask, which grants precise control of the cavity diameter and smooth edges as compared to a wet etch process. Simulations show

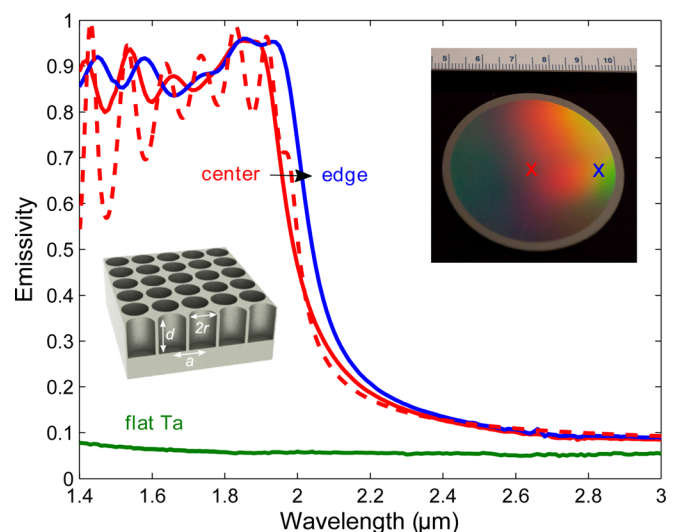


Fig. 5. (Color online) Measured room temperature emissivity of fabricated Ta PhC on 2 in. substrate measured in the center and towards the edge of the sample (solid lines) as compared to simulation (dashed line) and measured emissivity of flat Ta. Left inset: Schematic PhC structure. Right inset: Digital photo of the full 2 in. diameter sample after etching of the Cr hard mask; crosses indicate approximate measurement positions (scale is in cm).

that a random sidewall roughness leads to an increase of the emissivity and a trailing edge of the cutoff; therefore, smooth sidewalls are preferable. Also, we measured by Auger electron spectroscopy that there is no contamination from the Cr hard mask after removal of the etch mask, which would be detrimental to the desired low emissivity at long wavelengths.

Furthermore, a very good agreement with simulation results (as obtained from FDTD simulations) is achieved. Figure 5 compares the measured normal emissivity at room temperature to the simulated one. For the simulation, the radius $r = 0.53 \mu\text{m}$ and period $a = 1.33 \mu\text{m}$ as measured in the center of the fabricated 2 in. diameter Ta PhC and an etch depth of $d = 6.18 \mu\text{m}$ were used. As discussed above, the experimentally measured reflectance of the polished Ta substrates was used to establish a Drude–Lorentz model of the material, whose parameters incorporated in the simulation. As can be seen, the cut-off wavelength is precisely predicted by the simulation, and the measured cutoff is nearly as sharp as predicted. Small stochastic variations in the diameter of the fabricated cavities lead to some averaging of the emissivity below cutoff. Also, the measured emissivity above cutoff is as low as predicted by simulation.

The optical properties of the preannealed polished substrates were also characterized by the room temperature reflectivity measurement. The emissivity thus deduced is shown in Fig. 5 and is close to the emissivity of bulk Ta found in literature, demonstrating the optical quality of the polycrystalline Ta substrates. The thermal stability of nanostructured surfaces has been studied in few works.^{10,17,32} In these studies, it was reported that there is the risk of complete disintegration of the nanostructure, especially on polycrystalline materials, even after short times (1 h) at elevated temperatures. As reported, the structural deterioration is partly due to surface diffusion and partly due to recrystallization and grain migration. We used preannealed substrates, leading to large, stable grains, to approach these problems and increase the thermal stability of the nanostructures by providing a thermally stable substrate. Preliminary experimental results demonstrate the high-temperature stability of the PhC structures and their emissivity for 1 week at 910°C without any performance or structural degradation. In addition, we have performed multiple shorter time scale annealing tests, also at higher temperatures, showing that this is a promising route to thermal stability of nanostructured selective thermal emitters. Further evaluation of the long-term stability and high-temperature emission is under way.

IV. CONCLUSION

We have demonstrated highly selective emitters based on 2D Ta PhCs, suitable for high-temperature applications, e.g., in energy conversion. We have established a fabrication route for large-area, high aspect ratio photonic crystals achieving outstanding fabrication uniformity and accuracy across samples of 2 in. diameter. High-purity polycrystalline Ta substrates were used as a starting point and annealed at high temperatures to achieve large grains and minimize grain boundary diffusion at high temperatures, then lapped and

polished to an optical degree. PhCs comprising a square array of cylindrical cavities were fabricated on these polycrystalline Ta wafers of up to 2 in. diameter, using interference lithography and reactive ion etching techniques. We have developed a deep reactive ion etch process for Ta using an $\text{SF}_6/\text{C}_4\text{F}_8$ based Bosch process that enabled us to achieve up to $\sim 8.5 \mu\text{m}$ deep cavities with an aspect ratio of up to ~ 8 , with very steep sidewalls and outstanding selectivity of the etch toward the Cr hard etch mask. The fabrication of the Cr hard mask was optimized using RIE to achieve smooth sidewalls and eliminate random sidewall roughness as obtained from a chemical wet etch of Cr. The selective emitters fabricated by this method showed excellent spectral selectivity, enhancement of the emissivity below cut-off approaching unity, and a sharp cut-off between the high emissivity region and the low emissivity region, while maintaining the low intrinsic emissivity of bare Ta above the cut-off wavelength. Moreover, the experimental results show excellent agreement with numerical simulations.

These promising results demonstrate the efficiency and performance of selective emitters and absorbers based on 2D Ta PhCs. This work is leading the way to scale up high-temperature nanophotonic devices, facilitating cost-effective large-area, high performance applications in high-temperature solid-state energy conversion.

ACKNOWLEDGMENTS

The authors would like to thank Walker R. Chan for valuable discussions, Richard Kaszeta and Chris Munro (Creare) for support regarding substrate preparation, as well as James Daley at NSL (MIT) for film deposition, and Tim Savas for assistance and training in interference lithography. Fabrication of Ta PhCs was done in part at the Nanostructures Laboratory (NSL) at MIT and at the Center for Nanoscale Systems (CNS) at Harvard University, a member of the National Nanotechnology Infrastructure Network (NNIN), which is supported by the National Science Foundation under NSF Award No. ECS-0335765. This work was partially supported by the Army Research Office through the Institute for Soldier Nanotechnologies under Contract Nos. DAAD-19-02-D0002 and W911NF-07-D000. Y.X.Y. and M.S. were partially supported by the MIT S3TEC Energy Research Frontier Center of the Department of Energy under Grant No. DE-SC0001299. V.R. gratefully acknowledges funding by the Austrian Science Fund (FWF): J3161-N20.

¹M. Zenker, A. Heinzel, G. Stollwerck, J. Ferber, and J. Luther, *IEEE Trans. Electron Devices* **48**, 367 (2001).

²C. J. Crowley, N. A. Elkouh, S. Murray, and D. L. Chubb, *AIP Conf. Proc.* **746**, 601 (2005).

³V. M. Andreev, A. S. Vlasov, V. P. Khvostikov, O. A. Khvostikova, P. Y. Gazaryan, S. V. Sorokina, and N. A. Sadchikov, *J. Sol. Energy Eng.* **129**, 298 (2007).

⁴N. P. Sergeant, O. Pincon, M. Agrawal, and P. Peumans, *Opt. Express* **17**, 22800 (2009).

⁵N. P. Sergeant, M. Agrawal, and P. Peumans, *Opt. Express* **18**, 5525 (2010).

⁶I. Celanovic, F. O'Sullivan, M. Ilak, J. Kassakian, and D. Perreault, *Opt. Lett.* **29**, 863 (2004).

- ⁷F. O'Sullivan, I. Celanovic, N. Jovanovic, J. Kassakian, S. Akiyama, and K. Wada, *J. Appl. Phys.* **97**, 033529 (2005).
- ⁸D. Chester, P. Bermel, J. D. Joannopoulos, M. Soljacic, and I. Celanovic, *Opt. Express* **19**, A245 (2011).
- ⁹A. Heinzl, V. Boerner, A. Gombert, B. Bläsi, V. Wittwer, and J. Luther, *J. Mod. Opt.* **47**, 2399 (2000).
- ¹⁰H. Sai, Y. Kanamori, and H. Yugami, *Appl. Phys. Lett.* **82**, 1685 (2003).
- ¹¹H. Sai and H. Yugami, *Appl. Phys. Lett.* **85**, 3399 (2004).
- ¹²E. Rephaeli and S. Fan, *Appl. Phys. Lett.* **92**, 211107 (2008).
- ¹³I. Celanovic, N. Jovanovic, and J. Kassakian, *Appl. Phys. Lett.* **92**, 193101 (2008).
- ¹⁴M. Araghchini, Y. X. Yeng, N. Jovanovic, P. Bermel, L. A. Kolodziejski, M. Soljacic, I. Celanovic, and J. D. Joannopoulos, *J. Vac. Sci. Technol. B* **29**, 061402 (2011).
- ¹⁵Y. X. Yeng, M. Ghebrebrhan, P. Bermel, W. R. Chan, J. D. Joannopoulos, M. Soljacic, and I. Celanovic, *Proc. Natl. Acad. Sci. U.S.A.* **109**, 2280 (2012).
- ¹⁶P. Nagpal, D. P. Josephson, N. R. Denny, J. DeWilde, and D. J. Norris, *J. Mater. Chem.* **21**, 10836 (2011).
- ¹⁷K. A. Arpin, M. D. Losego, and P. Braun, *Chem. Mater.* **23**, 4783 (2011).
- ¹⁸P. Nagpal, S. E. Han, A. Stein, and D. J. Norris, *Nano Lett.* **8**, 3238 (2008).
- ¹⁹S. Y. Lin, J. Moreno, and J. G. Fleming, *Appl. Phys. Lett.* **83**, 380 (2003).
- ²⁰S. Y. Lin, J. G. Fleming, Z. Y. Li, I. El-Kady, R. Biswas, and K. M. Ho, *J. Opt. Soc. Am. B* **20**, 1538 (2003).
- ²¹V. Rinnerbauer, S. Ndao, Y. X. Yeng, W. R. Chan, J. J. Senkevich, J. D. Joannopoulos, M. Soljacic, and I. Celanovic, *Energy Environ. Sci.* **5**, 8815 (2012).
- ²²M. L. Schattenburg, R. J. Aucoin, and R. C. Fleming, *J. Vac. Sci. Technol. B* **13**, 3007 (1995).
- ²³T. A. Savas, M. L. Schattenburg, J. M. Carter, and H. I. Smith, *J. Vac. Sci. Technol. B* **17**, 4167 (1996).
- ²⁴M. E. Walsh, "On the design of lithographic interferometer and their application," Ph.D. thesis (MIT, Cambridge, 2004).
- ²⁵E. H. Anderson, "Fabrication and electromagnetic applications of periodic nanostructures," Ph.D. thesis (MIT, Cambridge, 1988).
- ²⁶M. L. Schattenburg, E. H. Anderson, and H. I. Smith, *Phys. Scr.* **41**, 13 (1990).
- ²⁷D. L. Chan, M. Soljacic, and J. D. Joannopoulos, *Opt. Express* **14**, 8785 (2006).
- ²⁸M. Ghebrebrhan, P. Bermel, Y. X. Yeng, I. Celanovic, M. Soljacic, and J. D. Joannopoulos, *Phys. Rev. A* **83**, 033810 (2011).
- ²⁹A. Taflov and S. C. Hagness, *Computational Electrodynamics: The Finite-Difference Time-Domain Method* (Artech House, Boston, 2000).
- ³⁰A. F. Oskooi, D. Roundy, M. Ibanescu, P. Bermel, J. Joannopoulos, and S. G. Johnson, *Comput. Phys. Commun.* **181**, 687 (2010).
- ³¹P. Bermel, M. Ghebrebrhan, M. Harradon, Y. X. Yeng, I. Celanovic, J. D. Joannopoulos, and M. Soljacic, *Nanoscale Res. Lett.* **6**, 549 (2011).
- ³²C. Schlemmer, J. Aschaber, V. Boerner, and J. Luther, *AIP Conf. Proc.* **653**, 164 (2003).